



A Percutaneous Catheter for *In Vivo* Hyperspectral Imaging of Cardiac Tissue: Challenges, Solutions and Future Directions

KENNETH ARMSTRONG,¹ CINNAMON LARSON,¹ HUDA ASFOUR,² TERRY RANSBURY,³
and NARINE SARVAZIAN ²

¹Nocturnal Product Development, LLC, 8128 Renaissance Pkwy #210, Durham, NC 27713, USA; ²Department of Pharmacology and Physiology, The George Washington University, 2300 Eye Street NW, Washington, DC 20037, USA; and ³LuxMed Systems, Inc, 124 Country Drive, Weston, MA 02493, USA

(Received 24 December 2019; accepted 30 June 2020)

Associate Editor James E. Moore oversaw the review of this article.

Abstract

Purpose—Multiple studies have shown that spectral analysis of tissue autofluorescence can be used as a live indicator for various pathophysiological states of cardiac tissue, including ischemia, ablation-induced damage, or scar formation. Yet today there are no percutaneous devices that can detect autofluorescence signals from inside a beating heart. Our aim was to develop a prototype catheter to demonstrate the feasibility of doing so.

Methods and Results—Here we summarize technical solutions leading to the development of a percutaneous catheter capable of multispectral imaging of intracardiac surfaces. The process included several iterations of light sources, optical filtering, and image acquisition techniques. The developed system included a compliant balloon, 355 nm laser irradiance, a high-sensitivity CCD, bandpass filtering, and image acquisition synchronized with the cardiac cycle. It enabled us to capture autofluorescence images from multiple spectral bands within the visible range while illuminating the endocardial surface with ultraviolet light. Principal component analysis and other spectral unmixing post-processing algorithms were then used to reveal target tissue.

Conclusion—Based on the success of our prototype system, we are confident that the development of ever more sensitive cameras, recent advances in tunable filters, fiber bundles, and other optical and computational components makes it possible to create percutaneous catheters capable of acquiring hyper or multispectral hypercubes, including those based on autofluorescence, in real-time. This opens the door for widespread use of this methodology for high-resolution

intraoperative imaging of internal tissues and organs—including cardiovascular applications.

Keywords—Autofluorescence, Atrial fibrillation, Catheter ablation, Hyperspectral imaging.

ABBREVIATIONS

AF	Atrial fibrillation
Auf-HSI	Autofluorescence hyperspectral imaging
CCD	Charged coupled device
LA	Left atrium
LCTF	Liquid crystal tunable filter
LED	Light emitting diode
NADH	Nicotinamide adenine dinucleotide
RF	Radiofrequency
UV	Ultraviolet Light

INTRODUCTION

The Clinical Need

In-surgery identification of an acutely damaged muscle is a holy grail of atrial fibrillation (AF) ablation procedures. AF is the most common cardiac arrhythmia affecting more than 2.3 million Americans.⁹ Its incidence rises with age, bringing the estimated lifetime risk of AF in the United States to 22–26%.²⁶ AF represents a major factor in morbidity associated with cardiac causes and their medical costs. In addition, untreated AF increases the risk of stroke by five times.

Address correspondence to Kenneth Armstrong, Nocturnal Product Development, LLC, 8128 Renaissance Pkwy #210, Durham, NC 27713, USA; Narine Sarvazian, Department of Pharmacology and Physiology, The George Washington University, 2300 Eye Street NW, Washington, DC 20037, USA. Electronic mail: kc@nocturnalpd.com, phynas@gwu.edu

Pharmacological options to treat AF include life-long regimens of anti-arrhythmic drugs and anticoagulants that can be effective for some patients. However, in many cases, AF remains unresponsive to drug therapy and there are compounding issues of life-long adherence to drug regimens and the possibility of interactions with medications taken for comorbid conditions. Therefore, in the last two decades minimally invasive surgical intervention using percutaneous ablation catheters became a mainstream option to treat AF.⁸ However, despite its demonstrated effectiveness in a significant number of treated patients, AF often returns within weeks or months after surgery. AF recurrence rates after a single catheter ablation procedure range from 30 to 50%,¹¹ often requiring repeated surgery. The main reason for AF recurrence is the remaining viability gaps between the lesions created to electrically isolate AF triggers. The employed electroanatomical mapping systems (EAMS) are extremely useful to monitor patterns of electrical activity,²⁴ yet they are not capable of pointing to a specific cause of electrical isolation. The latter may result from tissue necrosis, functional changes in reversibly injured cells, or temporary edema. In the case of edema, it subsides after a few weeks, potentially restoring electrical conduction. The spatial resolution of EAMS is also inferior to an optical means to observe the surface to be ablated (i.e., millimeters for electrical mapping vs. microns in the case of an optical approach). Thus, anatomical peculiarities or small islands of viable tissue can escape EAMS detection. A percutaneous device that provides for *in-vivo*, real-time visualization of acutely ablated tissue (as well as any scarred tissue from previous ablations to avoid re-ablating the same sites) can be of great help to improve the success rates of AF ablation procedures and minimize its complications.

Another important clinical target is an *in-vivo* identification of myocardial scars. Physiological assessment and visualization of myocardial scar tissue can be critically important for the treatment of ventricular and supraventricular arrhythmias by reducing surgical time and improving the effectiveness of cardiac ablation procedures.^{2,3,34} It can also help to improve future stem cell and other injection-based therapies to aid infarct repair.³⁶ Current non-invasive methods of imaging myocardial scar tissue include different modalities of cardiac MRI,^{2,4,27} PET,³⁴ and single photon emission computed tomography.^{17,30,31} These methods are effective pre-surgery means to visualize the bulk of the scar within the myocardial wall. Yet, they are poorly suited for high-resolution intraoperative surgical guidance. A direct, high-resolution view of the cardiac substrate to be ablated would be a preferred approach. Several minimally

invasive, catheter-based methods are currently being developed to address this clinical need. Among them intracardiac echocardiography,⁷ optical coherence tomography,^{15,42,43} photoacoustic imaging,^{10,22} infrared hyperspectral imaging^{32,37} and polarization spectroscopy-based¹ catheters. None of these techniques rely on a spectral analysis of tissue autofluorescence. Yet if the latter is implemented, it will have multiple advantages. First, it does not need contrast agents since it relies on intrinsic changes in tissue absorption, scattering, and endogenous autofluorescence. Second, it can be used to report multiple tissue states—normal unablated myocardium, ischemic myocardium with an induced rise in NADH levels, acutely injured myocardium with a near complete loss of NADH, or scar tissue with a buildup of highly fluorescent collagen once injured tissue heals.^{21,33} Importantly, in addition to capturing changes in the NADH or collagen levels, analysis of autofluorescence also reveals a buildup of protein-lipid oxidation products, the formation of lipofuscin and other pigments, and/or protein coagulation due to changes in light scattering.

The patient pool for minimally invasive cardiac surgeries will continue to increase because of a growing population demographic. In addition to diagnostic cardiologists and interventional radiologists, cardiothoracic surgeons and endovascular/vascular surgeons are performing catheter-based procedures in cath lab settings. This creates a compelling case to develop advanced imaging tools that can make intracardiac ablation and injection procedures safer and more efficient. To address this need, our team has been developing percutaneous imaging catheter systems capable of acquiring tissue autofluorescence profiles that can reveal the above mentioned clinical targets such as ablation lesion sites and/or scar tissue (Fig. 1).

Other Catheter Systems

Currently, there is only one commercial visualization catheter that can identify endocardial structures. CardioFocus provides a closed-ended balloon catheter, as part of its HeartLight® Endoscopic Ablation System.¹³ The visualization system provided by HeartLight® utilizes white light for illumination. Therefore, it is poorly suited to identify ablation sites since the endocardial collagen layer is also white and obscures damage to the muscle beneath it.³⁵ There are also fluorescence-based endoscopes that can be used for non-cardiac targets, including tumor resection or guided surgery.^{40,41} These devices combine the use of fluorescence imaging with the visible light imaging capabilities of a traditional endoscopic imaging system. Yet these devices are not designed for percutaneous access and are not suitable to operate in blood-

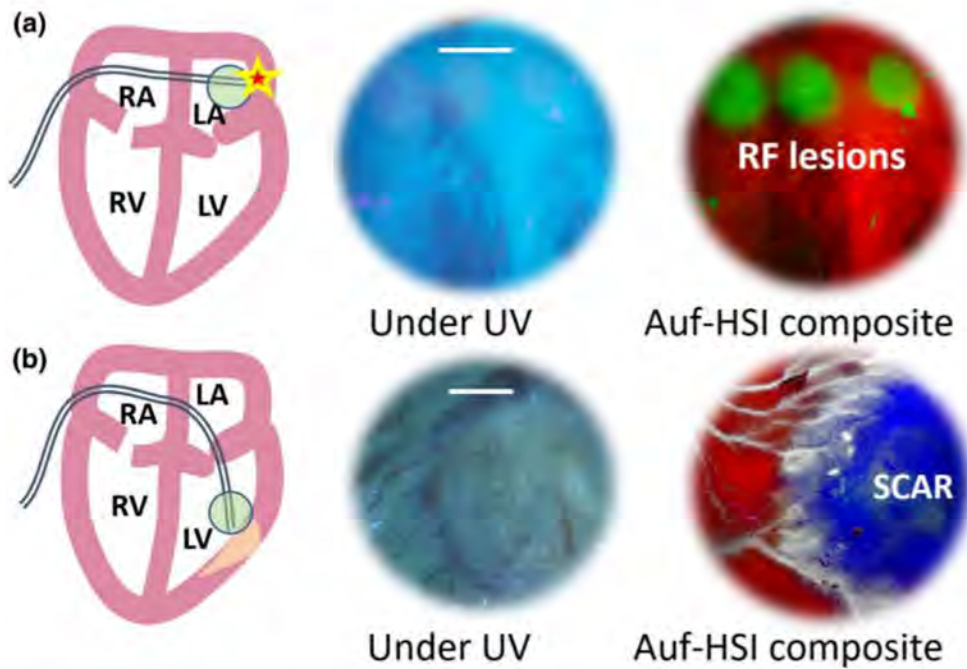


FIGURE 1. Envisioned imaging of cardiac targets using an Auf-HSI catheter. The illustrative images shown here are from our earlier bench studies including (a) excised porcine left atrium (details in Muselimyan *et al.*²⁸) and (b) excised rat heart ventricles (details in Swift *et al.*³⁶). The color map includes: green for lesion sites, red is healthy tissue, blue for scar, and white blood vessels. (a) On the left of the figure is a diagram depicting the catheter situated in the left pulmonary vein, which is common for AF ablation. The middle and right images are views of the ablated atrial surface. Middle image under UV and the right is an unmixed Auf-HSI composite. Scale bar—1 cm. (b) The same, but for ventricular scar visualization. Scale bar—2 mm.

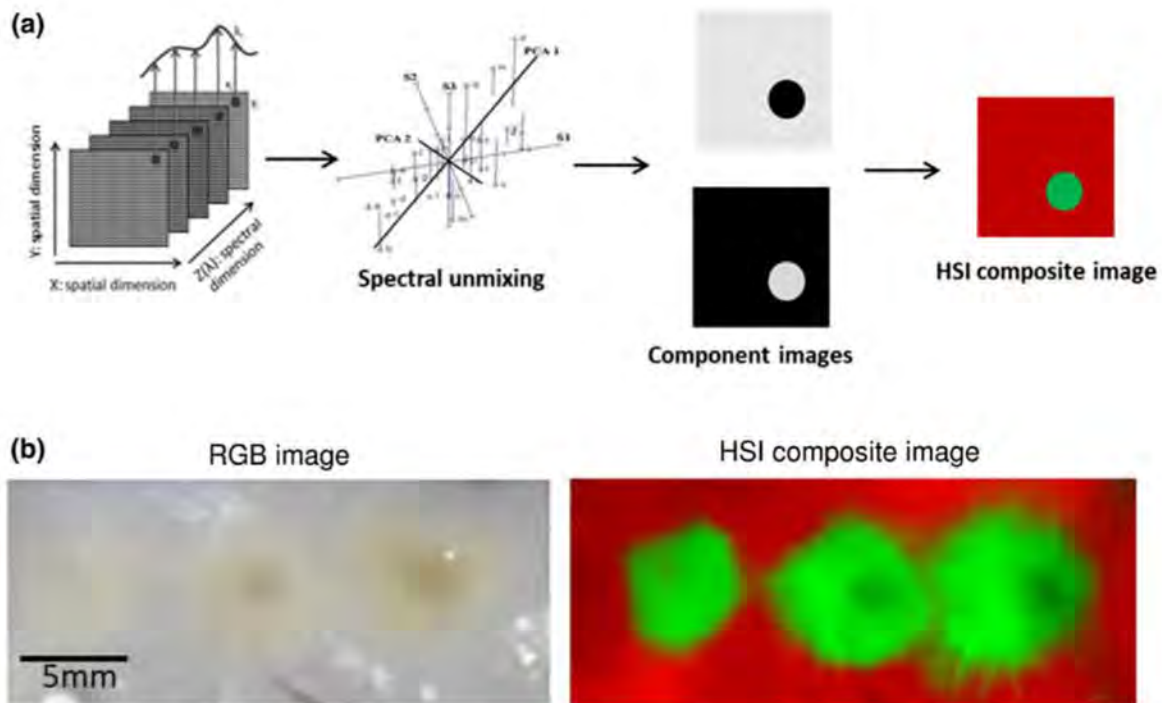


FIGURE 2. The concept of hyperspectral imaging. (a) From left to right: Multiple spectral planes are acquired to form a hypercube. Principal component analysis is used to create component images, which are then assigned pseudocolors and combined into a composite image. (b) Surface of ablated human left atrium under UV light as seen by a naked eye (left) and a pseudo colored composite image after Auf-HSI (right). These images were acquired from excised human tissue using Nuance FX hyperspectral camera and objective. Details of this experiment can be found in our earlier publication (Muselimyan *et al.*²⁸).

filed cavities of the beating heart. In addition, in most cases, they call for the injection of a fluorescing contrast agent.

Multispectral and Hyperspectral Imaging

These two imaging modalities combine the newest advances in optics and signal processing techniques to acquire and analyze spectra from each pixel of an image. It starts with the collection of individual images across many wavelengths under different illumination conditions. These images form a three-dimensional hyperspectral hypercube, with two spatial dimensions and one spectral dimension (Fig. 2). By definition, when the number of wavelengths is large enough to reconstruct a continuous spectrum, then such an imaging modality is commonly referred to as *hyperspectral imaging* (HSI). However, if the number of collected spectral wavelengths is discrete and the bands are wide and/or separated, it is then called *multispectral imaging*.

Spectra from each pixel are extracted and matched to existing spectral libraries or, alternatively, spectra are sorted using principal component analysis or other types of mathematical algorithms to reveal major spectral signatures in a sample.^{6,20} Based on the probability that the spectrum of an individual pixel matches a chosen target spectrum, a grey scale *component image* is then formed for each target. We create a *composite image* by combining two or more individual component images into a single image using pseudo colors. HSI and MSI are commonly used in art, geography, surveillance and material science to determine concentrations of different materials by comparing unknown spectra against pre-acquired spectral libraries.^{12,14,39} The use of these modalities biomedical applications is rapidly growing²⁵ and includes cancer detection, wound healing and image guided cancer surgery.^{16,23} Their potential benefits for surgical treatment of cardiac arrhythmias are numerous. They include: (i) immediate, in-surgery information about necrotic or ischemic tissue, (ii) identification of edema that may cause temporary electrical isolation, (iii) visualization of scar tissue in both atria and ventricles, (iv) finding the presence of fat, thrombi, calcifications, amyloid accumulation or fibrosis.

Here we would like to clarify our use of terms “hyper” vs. “multi”. Multispectral imagery generally refers to 3 to 10 bands, while hyperspectral imagery consists of hundreds of 10–20 nm bands from which continuous spectra can be extracted. All our bench, pre-catheter data were acquired using a Nuance FX system that collects continuous spectra from 420 to 720 nm with 2 to 10 nm resolution. That is why we use the term ‘hyperspectral’ when describing our findings. Our recent post-acquisition analysis of continuous

spectra from these hyperspectral datasets revealed the most informative wavelengths, allowing us to consider use of fewer and wider bands.^{6,19} In order not to confuse our readers by juggling between the two terms while referring to our previous publications and bench datasets, we decided to continue to refer to this technology as hyperspectral, although the final iteration of the clinical device is most likely to be classified as ‘multispectral’.

Hyperspectral Autofluorescence Imaging

Hyperspectral imaging based on tissue autofluorescence (Auf-HSI) is a subset of HSI. It employs illumination of the tissue surface with UV light while acquiring greyscale images across multiple spectral bands within the visible range. Autofluorescence spectra are then extracted from each pixel, sorted based on the differences in their normalized profiles, and assigned custom pseudocolors to reveal the desired targets. It is important to emphasize that by simply observing the image of cardiac surfaces under UV illumination one might not be able to visually distinguish the above-mentioned features. It is the post-acquisition processing algorithms that turn Auf-HSI into a powerful diagnostic tool by revealing the subtle changes in normalized spectral profiles from individual pixels (Fig. 2b). Without post-processing, the abundance of highly reflective and autofluorescent endocardial collagen tends to obscure either scars or ablation-induced tissue changes. Therefore, our team focused specifically on Auf-HSI. In addition, we have previously shown that for the identification of cardiac targets it is superior to HSI analysis based on reflected white light.⁵ To this end we have published several studies that demonstrated the ability of Auf-HSI to outline the boundaries of ablation sites in the atria of large mammals, including human tissue^{18,28,29} and to identify a myocardial scar.⁵ A number of potential advantages for the use of the Auf-HSI in clinical settings exist. When compared to the MRI, C-arm CT, and contrast echocardiography, Auf-HSI should be able to detect scar or ablation-induced structural changes without the need for contrast agents. While MRI and C-arm CT could take up to 30-min to visualize cell necrosis, Auf-HSI provides immediate feedback. When compared to echocardiography, Auf-HSI promises much better spatial resolution and a wider field-of-view. The latter is even truer when comparing Auf-HSI to optical coherence tomography (OCT), since catheter-based OCT does not inherently visualize over a wide-field.¹⁵

In the following sections, design considerations and technical challenges encountered during the development of percutaneous catheters suitable for the Auf-

HSI inside a beating heart are discussed for each of the catheter system's functionality.

CATHETER DESIGN—GENERAL CONSIDERATIONS

Transvenous cardiac catheterization procedures impose two basic physical restrictions – catheter diameter and catheter flexibility—that conspire to substantially limit optical throughput in an intracardiac imaging system. The primary components of the catheter used to perform imaging functions include an inflatable balloon that creates an optical window, a catheter body, and a catheter handle. Electrophysiology catheters for ablation and sensing are typically 7–8Fr (2.3–2.7 mm) in diameter, and 8–12fr-compatible steerable sheaths are most commonly used for transseptal procedures. Thus we constrained the maximum diameter of our balloon catheter to 10Fr (3.3 mm). The catheter body includes a pathway to deliver light to the tissue and a return pathway for induced fluoresced tissue response. There are also structural components to navigate the catheter to the target tissue and to provide stable contact during imaging. An additional port is required for the flow of saline that inflates the balloon. Note that while the catheter body itself is only 7.5Fr in diameter (2.5 mm), it is the distal tip of the catheter that determines the maximum catheter diameter of 10Fr, where the balloon is adhered to the outside surface of the catheter body. Ultimately, there is a trade-off between functionality, flexibility, and cross-sectional area of each component in the dimensional limits of the percutaneous catheter.

In their current configurations, the balloon catheter and RFA catheter will both fit in the left atrium (LA) at the same time. However, the balloon isn't intended to visualize the pulmonary vein during ablation, as doing so would compromise the irrigation performance of the RFA catheter, so the balloon catheter will be positioned in the pulmonary vein after the ablation catheter is withdrawn from direct contact with the ablated surface. Future evolution of the visualization catheter could incorporate electrodes on the balloon surface for ablation.

Below we present an overview of the tested catheter designs and outline possible solutions to overcome technical challenges for each optical component.

IMAGE ACQUISITION

Once space within the catheter body is allocated for pull wires for steering (or for a guidewire lumen for over-the-wire delivery) and fluid delivery, very little

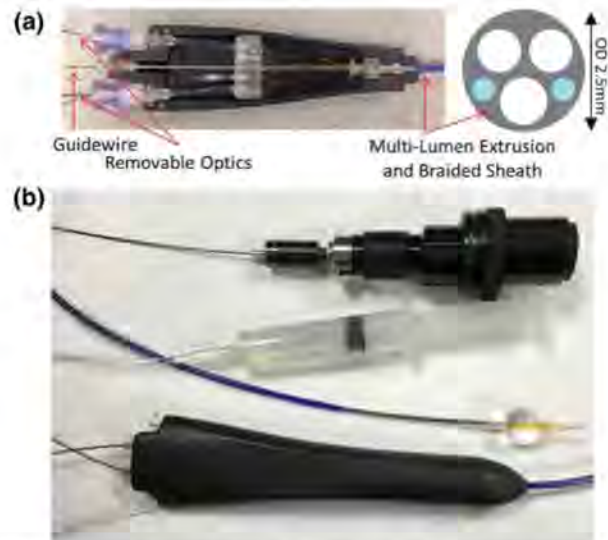


FIGURE 3. A prototype of Auf-HSI catheter. (a) Catheter handle with top cover removed. It shows two ports for insertable reusable optical fibers—one for light delivery and another for image acquisition. Isolated guidewire lumen allows for flushing and injection of contrast. Braided sheath provides torsional rigidity and column strength. (b) From top to bottom: Coupler to connect image fiber to camera C-mount, syringe with saline to fill the balloon, compliant custom-shaped balloon, catheter handle.

space remains for delivery of optical fibers to illuminate and acquire images (Fig. 3). On the illumination side, light must be delivered at the distal tip to irradiate the target tissue at energy levels sufficient for autofluorescence to be detected by optical sensors. On the detection side, the low light level of tissue autofluorescence must be collected using optical components with incredibly small apertures. Over the course of developing our prototypes, multiple irradiation and imaging approaches were attempted in order to optimize overall optical throughput and capture images of sufficient quality. In each case, special attention was given to the size and physical flexibility of potential solutions.

Microminiature CMOS Cameras

Advances in CMOS sensor technology has yielded extreme miniaturization of digital imaging systems, leading to the availability of cameras and integrated optics with diameters around 1 mm. The advantages of installing the entire imaging solution in the distal tip of the catheter are substantial. Catheter diameter would need only accommodate wires for camera power and communications, which would demand minimal space and would not notably impact flexibility. Unfortunately, the tested cameras, including single-photon devices, did not provide sufficient sensitivity to capture autofluorescence exhibited by cardiac tissue. They re-

main more suitable for reflectance-based imaging that involves white light illumination. Further, Auf-HSI requires the use of optical filtering in order to acquire spectral information for each pixel. This would require a tunable bandpass filter, which cannot be practically implemented in the distal tip of a 10Fr catheter using currently available technologies.

Coherent Imaging Bundle

An alternative solution is to place the camera and the filters at the proximal end of the catheter. This can be accomplished using coherent imaging bundles constructed from thousands of individual optical fibers organized into a structured array. The bundle is equipped with a lens at the distal end to focus the image onto the bundle face, and with optics at the proximal end that transfer the images from the bundle

to a camera. Imaging bundles are constructed with diameters of less than 1 mm and are commonly used in both medical and non-medical endoscopic imaging applications. The image guides used in our system were assembled by Zibra Corporation, using Fujikura FIGH-17-600G coherent imaging fibers. Each image guide comprises 17,000 individual fibers and together with the attached lens has an outer diameter of 0.8 mm (Fig. 4a). The spatial resolution is sufficient to observe lesions made by a standard clinical ablation catheters (Fig. 4b) allowing for a successful spectral unmixing (Fig. 4c). The assembled guide provides a 110-degree field of view in air, or 80-degree in saline (Fig. 5). The small diameter of this image guide makes it suitable for a 10Fr cardiac catheter. Its two main limitations are its limited bend radius of 30 mm, and the extremely small size of the lens. While the optics provide a very good depth of field (from 1 to 5 cm) their small size dramatically limits the amount of light available for imaging.

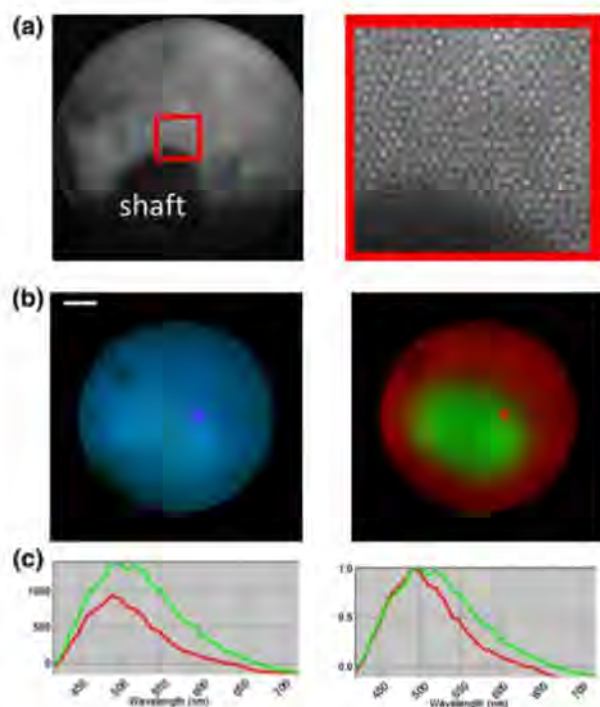


FIGURE 4. Input from the multifiber imaging guide. (a) Gray scale image of porcine atrial surface acquired *via* catheter with balloon shaft within the view (left). The magnified area from the red square shows input signals from individual fibers (right). (b) UV-illuminated surface of *ex vivo* porcine atrial endocardium as seen *via* multifiber imaging guide (left, RGB image, scale bar 1 mm). On the right is the outcome of the spectral unmixing of the corresponding 32-band hyperspectral dataset with red pseudocolor indicating the unablated tissue, green indicating an ablation lesion. (c) Raw (left) and normalized (right) spectra corresponding to the unablated (red) and ablated tissue shown in (b). Snapshots of the spectra as displayed by the Nuance FX HSI software interface (detailed unmixing protocol can be found in Gil *et al.*¹⁸).

TISSUE ILLUMINATION

Given the limited light-gathering capability of the imaging system, it is desirable to deliver as much UV irradiance to the tissue to be imaged as possible. Two approaches to deliver irradiation include sourcing the light at the distal tip of the catheter, or to producing it externally and delivering it to the distal tip *via* optical fiber.

Integrated Distal LEDs

One way to source irradiance at the tip of the catheter is to mount discrete UV LEDs on a flexible circuit substrate and deploy them into the balloon. The use of UV LEDs on this scale requires direct die-attach and wirebonding to a circuit substrate. We first tested this approach by prototyping it using a rigid format that was easier to assemble. The board included two white LEDs for visible-light imaging and 18 Fox 350 nm LED die. In total, this UV LED array yielded only 1.8 mW of optical power. When combined with the diffuse nature of the illuminating light, this was insufficient to elicit any measurable autofluorescence.

The next iteration of the LED array employed four Roithner 365 nm LEDs for a total radiant flux of 25 mW. Although this level of UV irradiance improved autofluorescence signals, the limited spectral purity of these LEDs made them unsuitable to perform HSI in the visible range. This is because the visible spectrum tail was comparable in magnitude to the tissue autofluorescence, thereby contaminating the image (Fig. 6a).

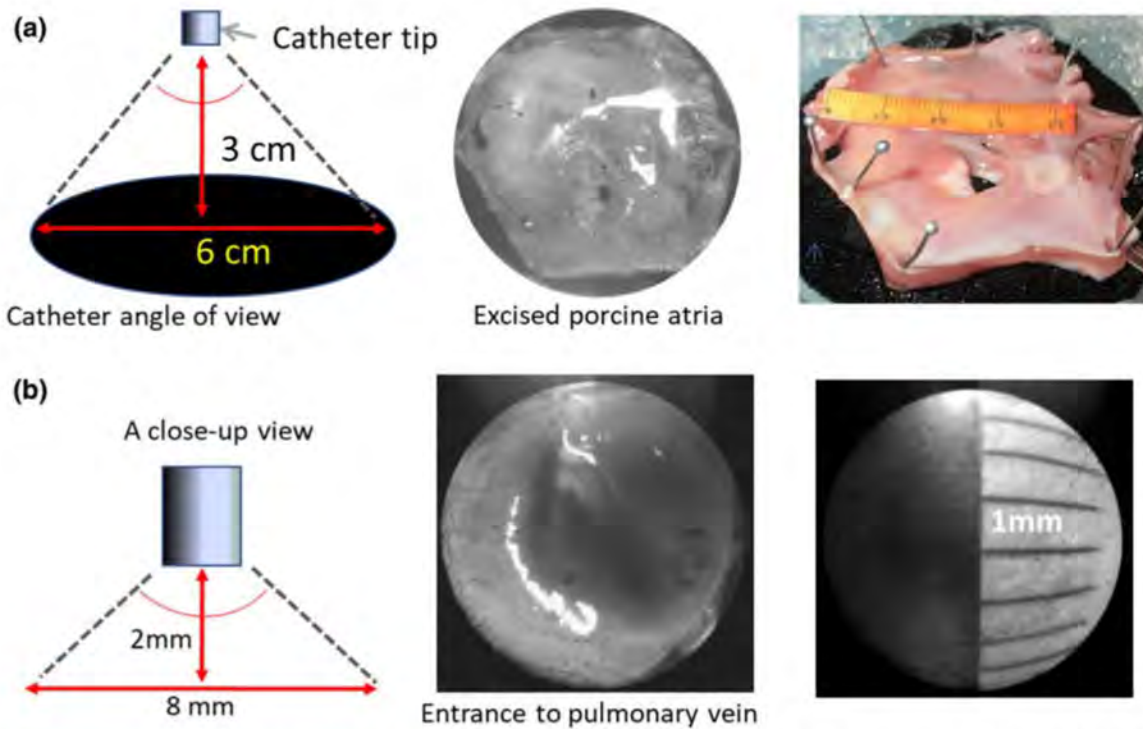


FIGURE 5. Field-of-view from the tip of imaging fiber. (a) At a distance of 3 cm from a surface, the field-of-view is about 6 cm. (b) At a closer distance, a fisheye effect becomes more evident.

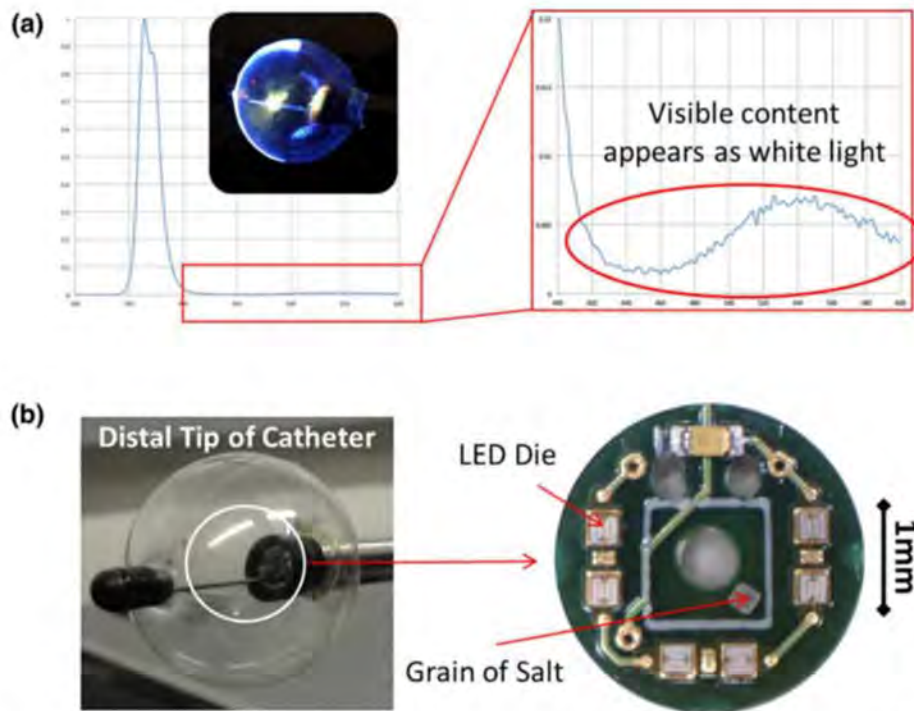


FIGURE 6. Use of UV LEDs for illumination. (a) Use of Roithner 365 nm LEDs yielded a poor contrast due to broadband, visible content in the LED spectrum, which overlapped with tissue autofluorescence signals. (b) Use of Roithner LED die wire-bonded to PCB on distal tip of 20Fr catheter. LEDs were synchronized with camera exposure *via* custom controller with an off-the-shelf, semi-compliant balloon.

The third option was to use LEDs from Sensor Electronic Technology, Inc (SETI) (Fig. 6b). These LEDs had both the power and spectral purity suitable for our application, but their commercial versions were provided in standard TO-39 packages, which at 8 mm in length and diameter were too large and SETI declined to source bare die. Therefore, the integrated LED architecture was abandoned in favor of an external light source.

External Light Sources

Based on prototype experience with distally mounted LEDs, it was evident that many milliwatts of total radiant flux is necessary to elicit tissue autofluorescence sufficient for Auf-HSI imaging. Due to the physics associated with the coupling of light into an optical fiber, it is not possible to inject this level of light into a small optical fiber using a diffuse light source, such as an LED. Thus it was necessary to use a coherent source, such as a laser, which could be focused entirely onto the diameter of the fiber. UV light delivery *via* optical fiber proved to be very challenging, with four iterations of the fiber-based light guide required to achieve sufficient optical throughput (Fig. 7). Another challenge for catheter-based imaging is the subsequent distribution of that light over the tissue surface. Fiber suitable for carrying UV is limited to 0.37NA at best, which corresponds to a 44° field of irradiance without additional optics. To increase that angle to 100°, a custom UV light guide was developed by Zibra Corporation that uses 0.22NA fiber and a custom lens assembly. As a source we used a Coherent Genesis CX laser that produces 110 mW of continuous

output at 355 nm. The coupling efficiency and losses within the light guide allowed for $\approx 50\%$ transmission efficiency, which permitted the delivery of > 50 mW of 355 nm irradiance to the tissue to be imaged.

Issues with Laser Speckle

The injection of laser light into a multi-mode fiber flattens the Gaussian intensity profile of the source beam, without reducing laser speckle. Incorporation of dynamic diffusers (Optotune, Dietikon, Switzerland) and the use of piezo elements to vibrate the optical fiber to change the speckle pattern at a rate above the integration time of the imaging system significantly reduced the undesirable speckle effect. However, while speckle was visually apparent when irradiating a smooth, uniformly fluorescent surface (Fig. 8), its impact was negligible when illuminating a highly variable myocardial surface. Furthermore, since the use of 17 k multimode fiber yields roughly a 130×130 pixel image, its low resolution is not sufficient to distinguish features as fine as the grain of the laser speckle. Therefore, given the limited utility of speckle reduction within the current prototype, it was eliminated to minimize the irradiance losses associated with its implementation.

Addressing Possible Dangers of UV Illumination

To the best of our knowledge there are no available published data regarding UV sensitivity of myocardium since there is no reason to think that such exposure would ever occur. The only available source of data regarding the effects of UV on living tissue are

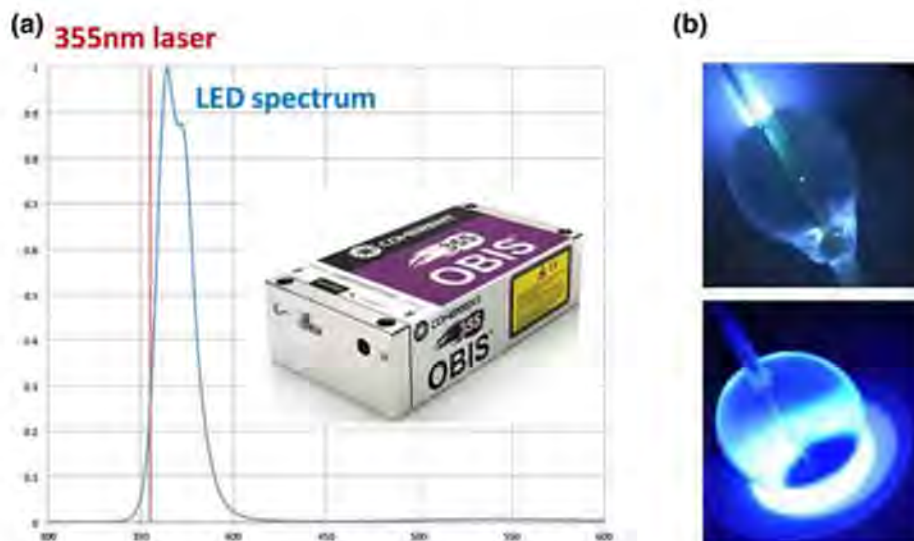
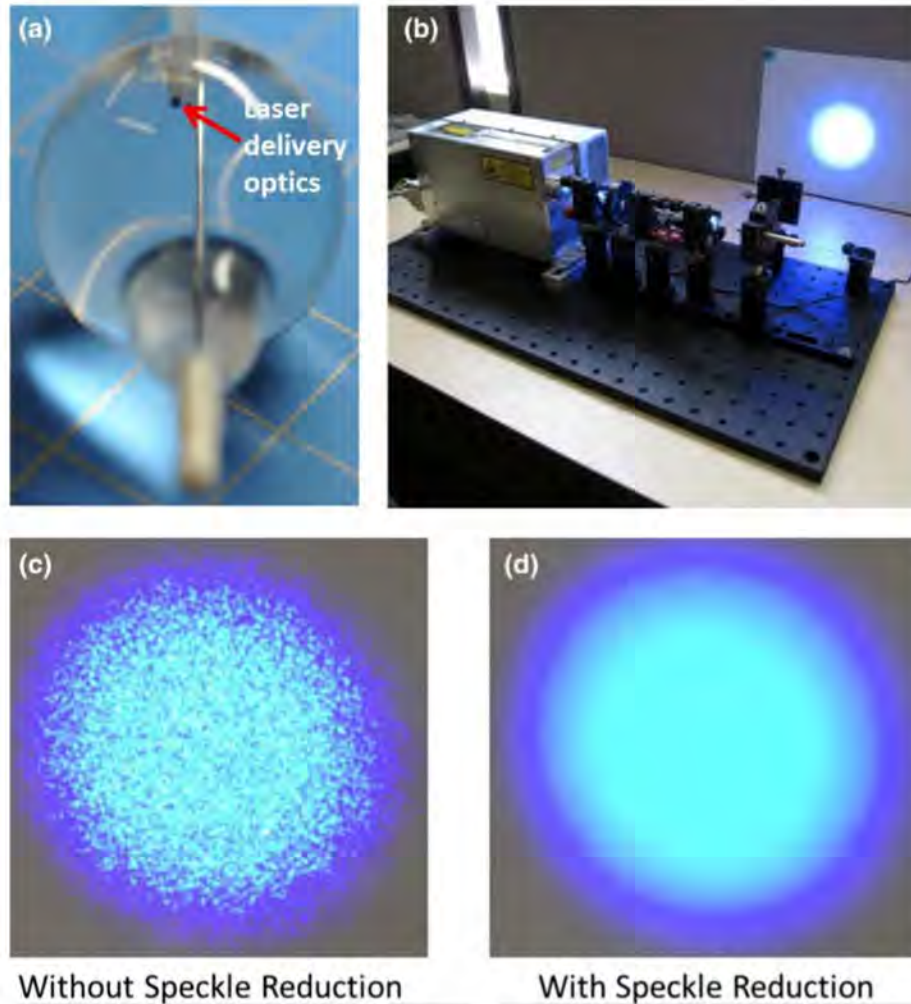


FIGURE 7. Use of 355 nm laser for illumination. (a) Spectra of Roithner LED vs. 355 nm OBIS Coherent laser. (b) Visual appearance of the balloon part of the catheter with partially inserted illumination fiber (top) vs. fully inserted fiber (bottom).



Without Speckle Reduction

With Speckle Reduction

FIGURE 8. Laser illumination and issue of laser speckle. (a) UV is delivered *via* a single 200-micron multimode optical fiber, utilizing a 300 μm sapphire lens assembly to spread the light onto the target tissue. (b) Bench testing setup of laser intensity and light distribution. (c, d) Use of a piezoelectric transducer to vibrate the laser delivery fiber minimizes the laser speckle.

the studies that involve skin. Ultraviolet radiation produces two adverse effects in skin tissue—erythema and photocarcinogenesis. Two standards established by CIE International Commission on Illumination standards specify action spectra for each of these effects: ISO 17166:1999 for the erythema, and ISO 28077:2006 for the photocarcinogenesis. These two standards summarize the findings of general photobiology literature regarding skin sensitivity to ultraviolet light. Our analysis of the irradiance at 355 to 365 nm using against these standards suggests that the levels of UV utilized for imaging are significantly lower than thresholds of UV that can damage the skin (See Appendix for detailed calculations).

It is important to also note that the range of wavelengths best suitable to elicit endogenous myocardial fluorescence is between 340 and 380 nm. This falls in what is called ‘soft UV’ or UVA range (315–400 nm). Compared to UVB or UVC, the UVA

exposure causes the least damage due to longer wavelength, which translates to lower photon energy.

HYPERSPECTRAL MODALITY TO REVEAL LESION FEATURES

In order to compose a hyperspectral dataset, one has to place a set of filters in front of the camera/sensor in order to collect individual images at different wavelengths. Our first approach relied on a commercial Nuance FX hyperspectral imaging system from PerkinElmer that uses an integrated liquid crystal tunable filter. The second approach utilized an Andor Ultra 897 camera coupled to a filter wheel with six discrete bandpass filters. For both approaches, the fiber image guide was connected *via* a custom C-mount coupler (Fig. 3b).

Nuance FX HSI System

The low optical throughput afforded by the limited UV irradiance available at the distal tip of the catheter, the low quantum efficiency of tissue autofluorescence, and the small aperture of the fiber image guide was further decreased due to the attenuation inherent to the liquid crystal tunable filter. To acquire a measurable number of photons, longer integration times were employed (up to 1 min) yielding good quality HSI data for immobilized or excised cardiac tissue. However, such low frame rates are incompatible with *in vivo* imaging of a beating heart. Thus, a systematic analysis was conducted to identify a few specific wavelengths that could be used to reveal the lesions without the necessity of acquiring high-resolution Auf-HSI datacubes.⁶ We were able to reduce the original hypercube consisting of 32 spectral images to a much smaller one comprising only 3–4 spectral images without a significant reduction in the ability of the unmixing algorithms to reveal the lesions. A smaller number of images within the cube allowed a dramatic reduction of the acquisition time of the hypercube. However, the sensitivity of the Nuance FX system was still not sufficient to produce hypercubes that can be acquired within the diastolic interval of a beating heart (200–300 ms).

Use of Filter Wheel and Gating

The critical wavelengths identified in our publications^{6,19} enabled the implementation of discrete filters in a filter wheel in place of a tunable filter (Fig. 9a). The use of discrete filters significantly increased the amount of light incident on the camera sensor, yet the integration times were still too long to fit into a diastolic window of 200–300 ms. To increase integration time, we developed custom gating hardware to monitor the body's surface electrogram and synchronize the camera and filter wheel with the heartbeat (Fig. 9b). The hardware analyzed the electrogram and triggered image acquisition in the time period between the T-wave and the next QRS complex. After exposure was complete, the hardware advanced the filter wheel during the QRS complex and T-wave so that the system would be prepared to image again prior to the next cardiac cycle. Using this synchronization method, the system was able to capture multiple successive images of cardiac tissue inside of a beating heart with sufficiently low integration time to produce usable data.

POSITIONING OF THE CATHETER

To be used in AF ablation procedures, the catheter must be maneuvered through the vasculature *via* a transfemoral approach, and into the left atrium *via* a

transseptal puncture in order to evaluate cardiac tissue before and after RF ablation. This can be accomplished either with a catheter that rides over a guidewire that is placed in the pulmonary veins transseptally, or with a catheter that incorporates a steering mechanism. We considered the advantages and drawbacks of both options.

Over-the-Wire Based Design

Guidewires for typical ablation catheters are 0.035 inches or 0.9 mm in diameter. The use of a 0.035" guidewire requires a lumen running the entire length of the catheter which spans approximately 1/3 of the 10Fr diameter. While this takes a large portion of available space, it is a simple lumen that does not require additional architecture to deliver the distal end of the catheter to the target location. In addition, over-the-guidewire catheters limit risk for puncturing the tissue since the catheter tip is riding over a wire and thus not contacting tissue surface directly. The use of a guidewire is a safe and easy access technique allowing for the catheter to be advanced through the vasculature to bring the optical window into contact with the ostia of the pulmonary veins. Moreover, since the catheter will be used to examine tissue before and after ablation, it is essential that the location of the optical window be the same before and after tissue is ablated. Using an over-the-wire delivery solution allows for the catheter to be placed for imaging of the tissue prior to ablating, retracted during ablation, and then returned to the same location post ablation. A guidewire delivery system thus ensures repeatable location of the catheter before and after lesion creation. However, there are three main drawbacks of guidewire-based catheter design. The first is that its positioning is limited to the location of the guidewire. The second is that the guidewire lumen runs through the optical window and thus obscures some of the visual path. And the third is that guidewire-based delivery is well-suited for targets around the ostia of pulmonary veins, but not necessarily for other intracardiac locations.

Steerable Design

There are two main upsides of steerable design: (1) the position of the catheter is not limited to the location of the guidewire, and (2) it allows for a balloon support structure that does not partially block the field of view (more below). On the other hand, a steerable design increases the complexity of the catheter and handle design. It also can increase the risk of a puncture of the catheter through the myocardium during the delivery procedure and catheter positioning. A steerable catheter will require pull wires to run the

Development of a Percutaneous Hyperspectral Catheter

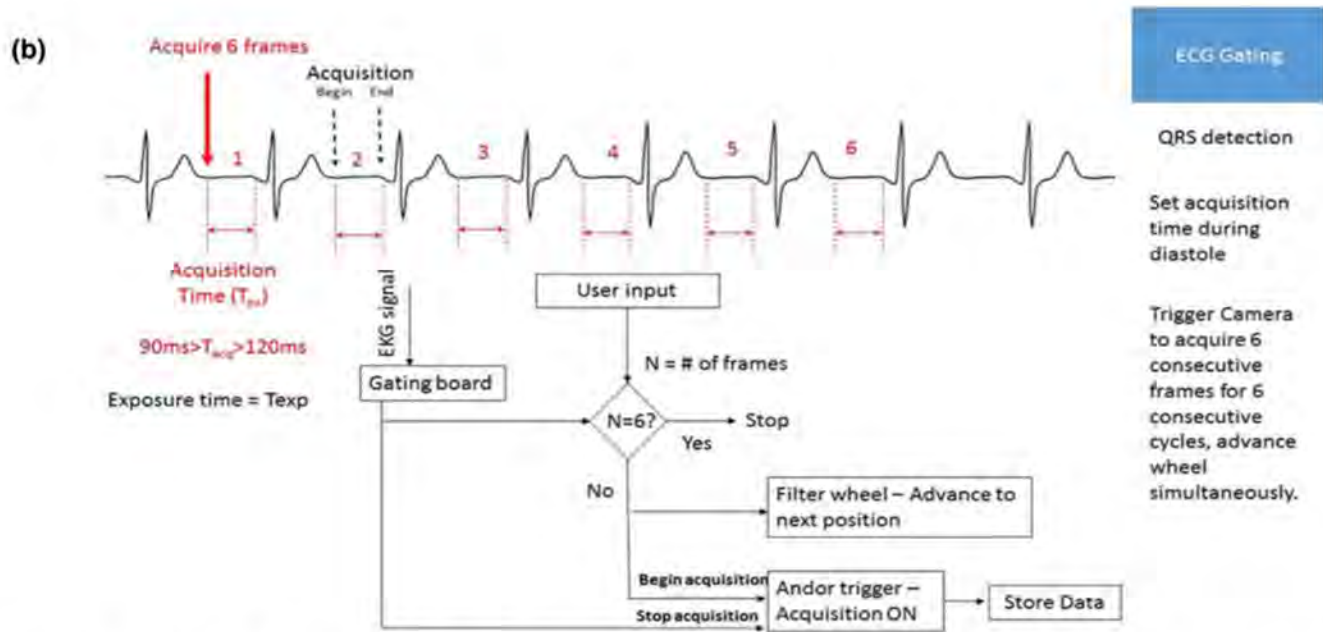
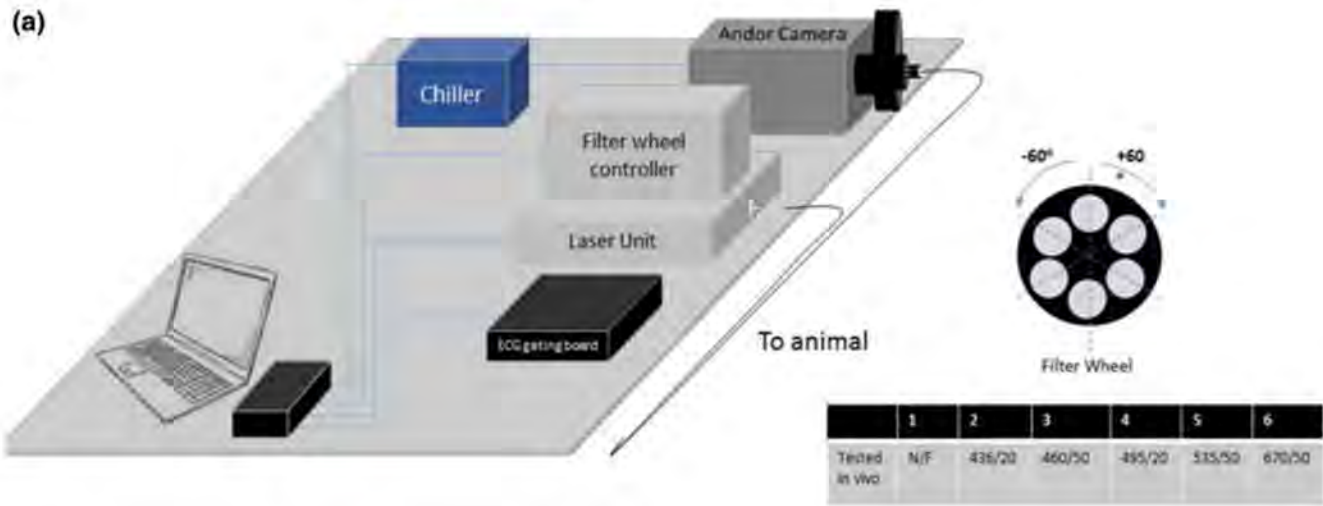


FIGURE 9. Use of filter wheel and ECG gating. (a) Hardware configuration that uses a filter wheel in front of the camera. (b) A diagram to illustrate how ECG gating was used to control filter wheel.

entire length of the catheter to a fixed structure, often a ring or laser cut hypotube, in the tip of the catheter. A structure called a fulcrum which transitions the stiffer portion of the catheter into a more flexible tip can provide the bend point for the catheter to deflect, allowing it to be steered to the target tissue location. The wires occupy less cross-sectional area of the catheter than the guidewire lumen previously discussed. However, the steering ring and fulcrum structures at the distal end would require a larger portion of the available cross-sectional area thus limiting the placement of other structures. In addition, returning to the exact location prior to removing the catheter with a

steerable system would likely require mapping capabilities which would increase overall complexity and require additional catheter space for the navigation sensor.

Stabilization and Maneuverability

Several other structural components are required in order to transmit both torque and axial force from the handle through the catheter shaft to the distal tip of the catheter. These structures are independent from any steering or over-the-wire capabilities and are essential to positioning the distal end of the catheter for illu-

mination and image acquisition. These structures are common to intravascular catheters and are composed of a stack of internal polymers, layered with structural coils or braids, and coated with polymer jackets. The internal architecture may be single lumens or a multi-lumen extrusion for delivery of the illumination and image guides, fluid, guidewire, or steering wires. The coil or braided structure is designed to transmit torque and axial force through the catheter body to the distal end of the catheter, thereby providing stability to the optical window and the ability to maneuver through a tortuous pathway to target tissue. Finally, the jacketing bonds the torque material and provides a smooth external surface to protect the vasculature along the delivery pathway of the catheter. These structures consume additional area from the 10Fr envelope of the catheter cross section. The materials and dimensions we used to date were comparable to commercially available 10Fr catheters with similar vasculature navigation requirements. Future efforts could include the use of improved materials (thinner wires and polymers) which still provide acceptable structural performance.

OPTICAL WINDOW

The distal portion of the catheter is comprised of an optical window which is realized as an expandable urethane balloon filled with saline. Once inside the left atrium, the balloon is inflated to a target diameter and then advanced to contact with the target pulmonary vein ostium to be imaged. The saline-filled balloon displaces the blood from the field of view and provides an optically clear window from the end of the optical guides in the catheter to the target tissue.

Saline-Based Inflation and Balloon Support

To date, we've made several custom-shaped balloons that can circumferentially contact the pulmonary vein ostium over a range of pulmonary vein sizes. The imaging optics are designed such that the field of view will cover the area of the balloon that contacts tissue at the largest possible vein size, and the depth of field extends from the nearest possible tissue location to beyond the tip of the balloon (Fig. 5). Image correction to account for fisheye effect seen in Fig. 5 could be easily implemented post acquisition by applying Fish-eye-Hemi from Imagio or any other commercial image processing filters. Interestingly, the need for such correction was not raised by users of other types of imaging catheters, such as the CardioFocus HeartLight.¹³

The custom-made balloons were molded from a medical grade urethane that can transform from a less

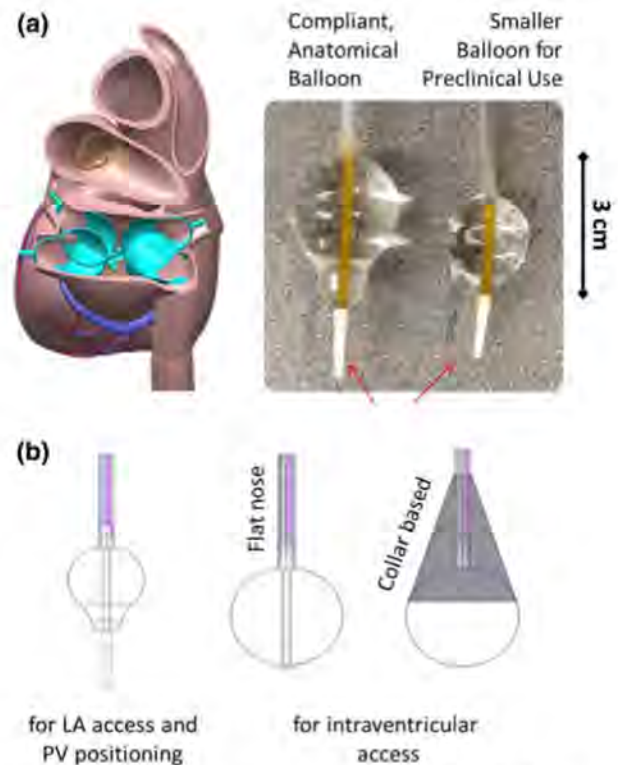


FIGURE 10. Custom balloons. (a) CAD model of PV anatomy, custom compliant urethane balloons designed to fit the pulmonary veins of human hearts (left) and porcine hearts (right). (b) Drawings of different balloon shapes for specific anatomical locations.

than 10Fr delivery/extraction diameter to a targeted expanded diameter of about 10–20 mm (Fig. 10a). The balloon structure adds to the catheter diameter on the distal end of the catheter only. However, two additional lumens running through the entire catheter structure are required for delivery and return of the saline to inflate and deflate the balloon. In order to keep fluid backpressure to reasonable levels, these lumens require only about 8% of the 10Fr cross-section. Once inflated, the balloon is pressed against the myocardial tissue to maximize the displacement of optically dense blood. In the current design, this is accomplished by the balloon being structurally supported by a guidewire running through the central axis of the balloon structure. The downside of such a design is a decreased field of view (Fig. 4a). In order to remove the central support structure from the balloon, an additional structure would have to be included to provide axial stability when the balloon is pressed against the myocardium for imaging and for stabilization of the surface during the cardiac cycle. This is because the compliant and flexible nature of the balloon prevents it from transmitting axial force from the catheter sufficient to maintain stability. Future catheter designs might include an expandable collar-like

support structure that can be deployed on the outside of the balloon to allow for axial load transmission while not obscuring the optical view. The ability to accomplish this type of support would allow for imaging of other endocardial tissue away from the PV ostium (Fig. 10b). Such a structure would still be required to fit within the 10Fr diameter and provide acceptable maneuverability.

Balloon Material

The material used to date was an ultra-compliant urethane ordered custom from Nordson Medical. Its advantages include its being atraumatic and safe on the cardiac surfaces and its ability to conform to the PV orifice without excessive displacement or distortion of tissue, which is a desirable procedural safety consideration. An additional increase of balloon pressure results in a larger diameter and increased field of view. The downside of this material is an autofluorescence profile that largely overlaps with tissue autofluorescence in both excitation and emission ranges, which significantly diminishes the ability of HSI to unmix autofluorescence spectra. Unfortunately, while searching for alternatives, we encountered a near complete lack of published information on the autofluorescence of polymers used for medical balloons. Therefore, we are currently examining several suitable balloon materials to identify polymers with improved fluorescent profiles for future iterations of the Auf-HSI catheter.

Other Issues

The use of UV light required special attention to material characteristics throughout the catheter. The entire assembly process ensured that no adhesives or other assembly materials were present anywhere in the optical path where they may contribute unwanted stray autofluorescence to the imaging data. This was of particular importance for structures within the field of view itself. Therefore, the central support structure of the balloon it was jacketed in polyamide in order to reduce its autofluorescence.

FUTURE DEVELOPMENTS

As discussed earlier, the primary limitation on system performance is optical throughput. It is influenced both by the available irradiance and by the light-gathering ability of the imaging system. As such, the most significant improvements in optical system performance of the device will result from advances in these areas.

Increasing Irradiance

Assuming the field of view is fixed, the only way to improve irradiance is to increase the amount of optical flux delivered to the tissue—be it LED or laser-based illumination. Advances in LED technology have provided high power density UV LEDs. SETi remains the best source for UV diodes, and while their off-the-shelf components provide substantial total power, they are currently too large to fit at the distal tip of a catheter. However, custom diodes or use of diode dies could potentially provide enough power in a smaller form. Increasing laser power is another likely path to success. When we started to develop our prototypes, 110 mW was the highest power level available for a 355 nm laser. Coherent now offers the same laser system at 250 mW. This will more than double the tissue irradiance from its current 4.5 to 10 mW/cm², and thus the total optical throughput of the system.

Image Acquisition

A few years ago, the Andor iXon 897 camera represented state-of-the-art technology. Based on the specifications of its successor—the Ultra 888—it appears that the notable improvement offered by the newer camera is higher resolution, and not improved sensitivity. Since our imaging resolution is limited by the pixel resolution of the fiber imaging bundle, increased sensor resolution, alone, would not improve system performance in any meaningful way. The best way to improve optical throughput on the imaging side is to increase the size of the imaging optics at the distal tip of the catheter. The most obvious implementation of this would be to increase the diameter of the fiber image guide and its distal lens assembly. The larger diameter optics would gather more light, thereby increasing overall optical throughput. The drawbacks to this are twofold: the first is a reduction in catheter flexibility, and the second is a decrease in available space inside the catheter body. The former could be addressed through the use of leached fiber bundles, which provide increased flexibility, though at a much higher cost. The latter, unfortunately, would need to be addressed by increasing catheter size—unless other components of the system are eliminated as discussed below. However, the past several years have seen an increase in the acceptable size of catheters used for atrial fibrillation treatment. The Medtronic Arctic Front cryoablation catheter, for example, now enjoys broad acceptance despite its 12Fr diameter. Though far less common than Arctic Front, CardioFocus' HeartLight catheter is similarly sized, and is also in use. The growing popularity of these newer catheters in spite of their large diameter in comparison with tra-

ditional 7–8Fr point ablation catheters suggests that the diameter of our Auf-HSI imaging catheter could increase to 12Fr with no market penalty. This increase in allowable maximum diameter would allow for the catheter extrusion to increase from 2.5 to 3.2 mm—providing considerably more space for optics as well as steering mechanics that might allow for changes in the distal tip to reduce the interference of balloon support structure with imaging field of view.

Removing Reusable Components

It is possible to increase the size of the distal imaging optics while maintaining the same fiber guide diameter. Doing so would eliminate the option of having the image guide be removable and reusable, dramatically increasing the cost of the catheter. This approach would also eliminate the option of over-the-wire delivery of the catheter, and would instead require the catheter to be steerable. This would not dramatically affect the usability of the catheter, but it would further increase the cost due to the added mechanical complexity in the catheter handle and body attendant with steerability.

Multifunctionality

Future improvements to the system could include dual functionality for each feature within the catheter. For example, the ability to use fixed optical guides that can provide structural rigidity or torque transmission along the length of the catheter could reduce the need for structural wire or coils in the catheter stackup. Cross sectional area of the lumens may then be reduced since the insertion and removal of these components would no longer be required. The current price of optical guide components makes such an improvement a costly proposition. However, it is possible that these components will become more affordable and could be disposed with the catheter body after each use. Alternatively, future efforts could be aimed at using structural components within the system to provide ablation therapy in addition to the imaging functionality, since market sensitivity to cost is considerably lower for therapeutic catheters as compared to diagnostic-only catheters. Another route could be adding HSI functionality to the currently available balloon-based system such as CardioFocus that employs a visible laser to ablate the tissue.

CONCLUSIONS

Using our current version of the catheter we were able to distinguish cardiac targets with large differences in their autofluorescence profiles both *ex vivo* (Figs. 4b and 4c) and *in vivo*.³⁸ However, long overall acquisition times (on the order of seconds for each spectral band) were required to visualize these targets, or spectral signatures were quite noisy. The catheter must be able to collect more light to improve its spectral unmixing capacity and to obtain images in a shorter amount of time since *in-vivo* movement of the heart severely constrains the acquisition times. Our bench data and all the technical improvements that we can foresee makes us confident that getting more light is an achievable goal. Improved optical throughput would reduce imaging noise by allowing for reduced camera sensor gain. While there is no specific target for throughput improvement, upgrading the laser alone could double the irradiance, which would allow for half the sensor gain with the same integration time. Increasing the diameter of the coherent imaging bundle would further improve the device's light gathering capability. Newer balloon materials should be used in place of autofluorescent urethane and our team was able to successfully identify such materials (Asfour *et al.*, in preparation). Lastly, a highly promising direction is to move to multispectral acquisition using fewer and wider spectral bands. Selection of such bands can be determined by computational analysis of comprehensive spectral information acquired using *ex vivo* hyperspectral imaging setups that are not subject to the above noted light limitations bands.^{6,19}

Hyperspectral and multispectral imaging provides the ability to greatly enhance the contrast between spectrally different components. In addition, it can reveal features otherwise invisible to a naked eye. The development of ever more sensitive cameras, recent advances in tunable filters, fiber bundles, and other optical and computational components makes it possible to envision percutaneous catheters capable of acquiring hyperspectral hypercubes, including the ones based on autofluorescence, in real-time. This opens the door for widespread use of this methodology for high-resolution intraoperative imaging of internal tissues and organs—including cardiovascular applications. Once fully developed, percutaneous hyper/multispectral catheters can also be used for non-cardiac surgeries or any diagnostic procedures in which there is limited visual contrast. Our team is truly excited about this technology and its clinical promise.

ELECTRONIC SUPPLEMENTARY MATERIAL

The online version of this article (<https://doi.org/10.1007/s13239-020-00476-w>) contains supplementary material, which is available to authorized users.

ACKNOWLEDGMENTS

We are thankful to our colleagues Drs. Omar Amirana and Narine Muselimyan for useful discussions, expert advice and experimental assistance.

CONFLICT OF INTEREST

Kenneth Armstrong: Employment: Nocturnal Product Development LLC. Funding: HL R41HL12051 & R42HL12051. Stock options: LuxMed Systems. Pending patents: US20150141847A1, US20160120599A1, US201361904018P, US20160143522A1. Granted patents: US9084611B2, US10143517B2. Terrance Ransbury: Employment: LuxMed Systems. Funding: HL R41HL12051 & R42HL12051. Stock options: LuxMed Systems. Pending patents: US20150141847A1, US20160120599A1, US201361904018P, US20160143522A1. Granted patents: US9084611B2, US10143517B2. Cinnamon Larson: Employment: NPD LLC. Funding: HL R41HL12051 & R42HL12051. Stock options: LuxMed Systems. Pending patents: US20150141847A1, US20160120599A1, US201361904018P, US20160143522A1. Granted patents: US9084611B2, US10143517B2. Huda Asfour: Employment: The George Washington University. Funding: HL R41HL12051 & R42HL12051. Narine Sarvazyan: Employment: The George Washington University. Funding: HL R41HL12051 & R42HL12051. Stock options: LuxMed Systems. Pending patents: US20150141847A1, US20160120599A1, US201361904018P. Granted patents: US9014789B2, US9084611B2.

REFERENCES

- ¹Ahmad, I., A. Gribble, M. Ikram, M. Pop, and A. Vitkin. Polarimetric assessment of healthy and radiofrequency ablated porcine myocardial tissue. *J. Biophotonics* 9:750–759, 2016.
- ²Akoum, N., M. Daccarett, C. McGann, N. Segerson, G. Vergara, S. Kuppahally, T. Badger, N. Burgon, T. Haslam, E. Kholmovski, R. Macleod, and N. Marrouche. Atrial fibrosis helps select the appropriate patient and strategy in catheter ablation of atrial fibrillation: a DE-MRI guided approach. *J. Cardiovasc. Electrophysiol.* 22:16–22, 2011.
- ³Aldhoon, B., T. Kučera, N. Smorodinová, J. Martinek, V. Melenovský, and J. Kautzner. Associations between cardiac fibrosis and permanent atrial fibrillation in advanced heart failure. *Physiol. Res.* 62:247–255, 2013.
- ⁴Andreu, D., A. Berruezo, J. T. Ortiz-Pérez, E. Silva, L. Mont, R. Borrás, T. M. de Caralt, R. J. Perea, J. Fernández-Armenta, H. Zeljko, and J. Brugada. Integration of 3D electroanatomic maps and magnetic resonance scar characterization into the navigation system to guide ventricular tachycardia ablation clinical perspective. *Circ. Arrhythm. Electrophysiol.* 4:674–683, 2011.
- ⁵Asfour, H., M. Aljishi, T. Chahbazian, L. M. Swift, N. Muselimyan, D. Gil, and N. A. Sarvazyan. Comparison between autofluorescence and reflectance-based hyperspectral imaging for visualization of atrial ablation lesions. *Biophys. J.* 110:493a–494a, 2016.
- ⁶Asfour, H., S. Guan, N. Muselimyan, L. Swift, M. Loew, and N. Sarvazyan. Optimization of wavelength selection for multispectral image acquisition: a case study of atrial ablation lesions. *Biomed. Opt. Express* 9:2189–2204, 2018.
- ⁷Bunch, T. J., J. P. Weiss, B. G. Crandall, J. D. Day, J. P. Dimarco, J. D. Ferguson, P. K. Mason, G. McDaniel, J. S. Osborn, D. Wiggins, and S. Mahapatra. Image integration using intracardiac ultrasound and 3D reconstruction for scar mapping and ablation of ventricular tachycardia. *J. Cardiovasc. Electrophysiol.* 21:678–684, 2010.
- ⁸Calkins, H., G. Hindricks, R. Cappato, Y. H. Kim, E. B. Saad, L. Aguinaga, J. G. Akar, V. Badhwar, J. Brugada, J. Camm, P. S. Chen, S. A. Chen, M. K. Chung, J. C. Nielsen, A. B. Curtis, D. W. Davies, J. D. Day, A. d'Avila, N. M. S. Natasja de Groot, L. Di Biase, M. Duytschaever, J. R. Edgerton, K. A. Ellenbogen, P. T. Ellinor, S. Ernst, G. Fenelon, E. P. Gerstenfeld, D. E. Haines, M. Haissaguerre, R. H. Helm, E. Hylek, W. M. Jackman, J. Jalife, J. M. Kalman, J. Kautzner, H. Kottkamp, K. H. Kuck, K. Kumagai, R. Lee, T. Lewalter, B. D. Lindsay, L. Macle, M. Mansour, F. E. Marchlinski, G. F. Michaud, H. Nakagawa, A. Natale, S. Nattel, K. Okumura, D. Packer, E. Pokushalov, M. R. Reynolds, P. Sanders, M. Scavacca, R. Schilling, C. Tondo, H. M. Tsao, A. Verma, D. J. Wilber, and T. Yamane. 2017 HRS/EHRA/ECAS/APHRS/SOLAECE expert consensus statement on catheter and surgical ablation of atrial fibrillation: Executive summary. *Heart Rhythm* 33(5):369–409, 2017.
- ⁹Cappato, R., H. Calkins, S.-A. A. Chen, W. Davies, Y. Iesaka, J. Kalman, Y.-H. H. Kim, G. Klein, A. Natale, D. Packer, A. Skanes, F. Ambrogi, and E. Biganzoli. Updated worldwide survey on the methods, efficacy, and safety of catheter ablation for human atrial fibrillation. *Circ. Arrhythm. Electrophysiol.* 3:32–38, 2010.
- ¹⁰Dana, N., L. Di Biase, A. Natale, S. Emelianov, and R. Bouchard. In vitro photoacoustic visualization of myocardial ablation lesions. *Heart Rhythm* 11:150–157, 2013.
- ¹¹Deng, H., Y. Bai, A. Shantsila, L. Fauchier, T. S. Potpara, and G. Y. H. Lip. Clinical scores for outcomes of rhythm control or arrhythmia progression in patients with atrial fibrillation: a systematic review. *Clin. Res. Cardiol.* 106(10):813–823, 2017.
- ¹²Dooley, K. A., S. Lomax, J. G. Zeibel, C. Miliani, P. Ricciardi, A. Hoenigswald, M. H. Loew, and J. K. Delaney. Mapping of egg yolk and animal skin glue paint binders in Early Renaissance paintings using near infrared reflectance imaging spectroscopy. *Analyst* 138:4838–4848, 2013.
- ¹³Dukkipati, S. R., F. Cuoco, I. Kutinsky, A. Aryana, T. D. Bahnson, D. Lakkireddy, I. Woollett, Z. F. Issa, A. Natale, and V. Y. Reddy. Pulmonary vein isolation using the visually guided laser balloon. *J. Am. Coll. Cardiol.* 66:1350–1360, 2015.

- ¹⁴Falco, N. An ICA based approach to hyperspectral image feature reduction. In: *Geoscience Remote*, 2014.
- ¹⁵Fleming, C. P., H. Wang, K. J. Quan, and A. M. Rollins. Real-time monitoring of cardiac radio-frequency ablation lesion formation using an optical coherence tomography forward-imaging catheter. *J. Biomed. Opt.* 15:030516, 2010.
- ¹⁶Gaudi, S., R. Meyer, J. Ranka, J. C. Granahan, S. A. Israel, T. R. Yachik, and D. M. Jukic. Hyperspectral imaging of melanocytic lesions. *Am. J. Dermatopathol.* 36(2):131–136, 2014.
- ¹⁷Germano, G., and D. S. Berman. *Clinical Gated Cardiac SPECT*. Armonk: Blackwell Futura, 2006.
- ¹⁸Gil, D. A., L. M. Swift, H. Asfour, N. Muselimyan, M. A. Mercader, and N. A. Sarvazyan. Autofluorescence hyperspectral imaging of radiofrequency ablation lesions in porcine cardiac tissue. *J. Biophotonics* 10:1008–1017, 2017.
- ¹⁹Guan, S., H. Asfour, N. Sarvazyan, and M. Loew. Application of unsupervised learning to hyperspectral imaging of cardiac ablation lesions. *J. Med. Imaging* 5:1, 2018.
- ²⁰Guan, S., M. Loew, H. Asfour, N. Sarvazyan, and N. Muselimyan. Lesion detection for cardiac ablation from auto-fluorescence hyperspectral images. In: *Progress in Biomedical Optics and Imaging—Proceedings of SPIE*, 2018, Vol. 10578.
- ²¹Holmes, J. W., T. K. Borg, and J. W. Covell. Structure and mechanics of healing myocardial infarcts. *Annu. Rev. Biomed. Eng.* 7:223–253, 2005.
- ²²Iskander-Rizk, S., P. Kruizinga, A. F. W. van der Steen, and G. van Soest. Spectroscopic photoacoustic imaging of radiofrequency ablation in the left atrium. *Biomed. Opt. Express* 9:1309–1322, 2018.
- ²³Kiyotoki, S., J. Nishikawa, T. Okamoto, K. Hamabe, M. Saito, A. Goto, Y. Fujita, Y. Hamamoto, Y. Takeuchi, S. Satori, and I. Sakaida. New method for detection of gastric cancer by hyperspectral imaging: a pilot study. *J. Biomed. Opt.* 18:26010, 2013.
- ²⁴Lo, L.-W. W., and S.-A. A. Chen. Three-dimensional electroanatomic mapping systems in catheter ablation of atrial fibrillation. *Circ. J.* 74:18–23, 2010.
- ²⁵Lu, G., and B. Fei. Medical hyperspectral imaging: a review. *J. Biomed. Opt.* 19:10901, 2014.
- ²⁶Magnani, J. W., M. Rienstra, H. Lin, M. F. Sinner, S. A. Lubitz, D. D. McManus, J. Dupuis, P. T. Ellinor, and E. J. Benjamin. Atrial fibrillation: current knowledge and future directions in epidemiology and genomics. *Circulation* 124(18):1982–1993, 2011.
- ²⁷McGann, C. J., E. G. Kholmovski, R. S. Oakes, J. J. E. Blauer, M. Daccarett, N. Segerson, K. J. Airey, N. Akoum, E. Fish, T. J. Badger, E. V. R. DiBella, D. Parker, R. S. MacLeod, and N. F. Marrouche. New magnetic resonance imaging-based method for defining the extent of left atrial wall injury after the ablation of atrial fibrillation. *J. Am. Coll. Cardiol.* 52:1263–1271, 2008.
- ²⁸Muselimyan, N., M. Al Jishi, H. Asfour, L. Swift, and N. A. Sarvazyan. Anatomical and optical properties of atrial tissue: search for a suitable animal model. *Cardiovasc. Eng. Technol.* 8:505–514, 2017.
- ²⁹Muselimyan, N., L. M. Swift, H. Asfour, T. Chahbazian, R. Mazhari, M. Mercader, and N. A. Sarvazyan. Seeing the invisible: revealing atrial ablation lesions using hyperspectral imaging approach. *PLoS ONE* 11:e0167760, 2016.
- ³⁰Nazarian, S., and R. Beinart. CMR-guided targeting of gaps after initial pulmonary vein isolation. *JACC. Cardiovasc. Imaging* 7:664–666, 2014.
- ³¹Nelson, C., J. McCrohon, F. Khafagi, S. Rose, R. Leano, and T. H. Marwick. Impact of scar thickness on the assessment of viability using dobutamine echocardiography and thallium single-photon emission computed tomography. *J. Am. Coll. Cardiol.* 43:1248–1256, 2004.
- ³²Park, S. Y., R. P. Singh-Moon, E. Y. Wan, and C. P. Hendon. Towards real-time multispectral endoscopic imaging for cardiac lesion quality assessment. *Biomed. Opt. Express* 10(6):2829–2846, 2019.
- ³³Prabhu, S. D., and N. G. Frangogiannis. The biological basis for cardiac repair after myocardial infarction. *Circ. Res.* 119:91–112, 2016.
- ³⁴Rijnierse, M. T., C. P. Allaart, and P. Knaapen. Principles and techniques of imaging in identifying the substrate of ventricular arrhythmia. *J. Nucl. Cardiol.* 23:218–234, 2016.
- ³⁵Schade, A., J. Krug, A.-G. Szöllösi, M. El Tarahony, and T. Deneke. Pulmonary vein isolation with a novel endoscopic ablation system using laser energy. *Expert Rev. Cardiovasc. Ther.* 10:995–1000, 2012.
- ³⁶Shiba, Y., S. Fernandes, W.-Z. Zhu, D. Filice, V. Muskheli, J. Kim, N. J. Palpant, J. Gantz, K. W. Moyes, H. Reinecke, B. Van Biber, T. Dardas, J. L. Mignone, A. Izawa, R. Hanna, M. Viswanathan, J. D. Gold, M. I. Kotlikoff, N. A. Sarvazyan, M. W. Kay, C. E. Murry, and M. A. Laflamme. Human ES-cell-derived cardiomyocytes electrically couple and suppress arrhythmias in injured hearts. *Nature* 489:332–335, 2012.
- ³⁷Singh-Moon, R. P., C. C. Marboe, and C. P. Hendon. Near-infrared spectroscopy integrated catheter for characterization of myocardial tissues: preliminary demonstrations to radiofrequency ablation therapy for atrial fibrillation. *Biomed. Opt. Express* 6:2494, 2015.
- ³⁸Swift, L. M., H. Asfour, N. Muselimyan, C. Larson, K. Armstrong, and N. A. Sarvazyan. Hyperspectral imaging for label-free in vivo identification of myocardial scars and sites of radiofrequency ablation lesions. *Heart Rhythm* 15:564–575, 2018.
- ³⁹Tarabalka, Y., J. A. Benediktsson, and J. Chanussot. Spectral–spatial classification of hyperspectral imagery based on partitional clustering techniques. *IEEE Trans. Geosci. Remote Sens.* 47:2973–2987, 2009.
- ⁴⁰Tate, T. H., M. Keenan, J. Black, U. Utzinger, and J. K. Barton. Ultraminiature optical design for multispectral fluorescence imaging endoscopes. *J. Biomed. Opt.* 22(3):036013, 2017.
- ⁴¹Tsutsui, N., M. Yoshida, E. Ito, H. Ohdaira, M. Kitajima, and Y. Suzuki. Laparoscopic cholecystectomy using the PINPOINT® Endoscopic Fluorescence Imaging System with intraoperative fluorescent imaging for acute cholecystitis: a case report. *Ann. Med. Surg.* 35:146–148, 2018.
- ⁴²Zhao, X., X. Fu, C. Blumenthal, Y. T. Wang, M. W. Jenkins, C. Snyder, M. Arruda, and A. M. Rollins. Integrated RFA/PSOCT catheter for real-time guidance of cardiac radio-frequency ablation. *Biomed. Opt. Express* 9(12):6400–6411, 2018.
- ⁴³Zhao, X., O. Kilinc, C. J. Blumenthal, D. Dosluoglu, M. W. Jenkins, C. S. Snyder, M. Arruda, and A. M. Rollins. Intracardiac radiofrequency ablation in living swine guided by polarization-sensitive optical coherence tomography. *J. Biomed. Opt.* 25(5):056001, 2020.

Publisher's Note Springer Nature remains neutral with regard to jurisdictional claims in published maps and institutional affiliations.

APPENDIX A: DETAILED ERYTHEMA ANALYSIS

The basic, driving characteristics of the optical system pertaining to illumination exposure are:

Excitation wavelength, fiber diameter, and emitted laser power at the distal tip of the catheter:

$$\lambda_{ex} = 355nm$$

$$r_{FOI} = 2cm \cdot \tan(40^\circ) = 1.68cm$$

$$P_{LASER} = 250mW \cdot 60\% = 150mW$$

The total irradiance at the tissue is defined by the laser power and the area over which it is distributed.

$$A_C = \pi \cdot (r_{FOI})^2 = 8.85cm^2$$

$$E_{UV} = \frac{P_{LASER}}{A_C} = 17 \frac{mW}{cm^2} = 170 \frac{W}{m^2}$$

Per ISO 17166:1999, the erythema reference action spectrum for UVA radiation (315nm - 400nm) is defined as $S_{er}(\lambda) = 10^{0.015(140 - \lambda)}$, where λ is in nm.

$$S_{er}(\lambda) = 10^{0.015(140 - \lambda)} = 0.000596$$

One erythemal quantity is defined as

$$\Phi = 100 \frac{J}{m^2}$$

The erythemal dose over a period of t seconds is defined, in *standard erythemal dose*, or SED, as

$$H_{er}(t) = \frac{E_{UV} \cdot S_{er}(\lambda_{ex}) \cdot t}{\Phi}$$

Rearranging this equation to solve for time as a function of SED gives

$$t_{exp}(SED) = \frac{SED \cdot \Phi}{E_{UV} \cdot S_{er}(\lambda_{ex})}$$

The ISO 17166:1999 action spectrum is normalized to 298nm, at which wavelength, per CIE 106:1993, the *minimum erythemal dose*, or MED, is $350-430 \frac{J}{m^2}$ (p.16, Table 1). This equates to 3.5 to 4.3 SED.

Per ISO 17166, Fitzpatrick skin types (phototypes) I - IV would encompass a range of 1.5 to 6 SED. Using the minimum value for the most sensitive skin phototype yields:

$$t_{exp}(1.5) = \frac{1.5 \cdot 100 \frac{W}{m^2}}{170 \frac{W}{m^2} \cdot 0.000596} = 1,480 \text{ sec}$$

Thus, a CIE 106 MED of 1.5 equates to an exposure time of 1,480 seconds, or almost 25 minutes if myocardium is assumed to be as sensitive to 355nm irradiance as the most sensitive of skin types. Since imaging of a pulmonary vein will require an order of magnitude less time than this, myocardium exposure to 355nm should not result in any tissue damage.